

The origin of chemical inhomogeneity in lead-free potassium sodium niobate ceramic: competitive chemical reaction during solid-state synthesis

Hao-Cheng Thong,^{1,#} Alexis Payne,^{2,#} Jia-Wang Li,¹ Yue-Yu-Shan Cheng,¹
Jacob L. Jones^{2,*}, and Ke Wang,^{1,*}

¹ State Key Laboratory of New Ceramics and Fine Processing, School of Materials Science and Engineering, Tsinghua University, Beijing 100084, China.

² Department of Materials Science and Engineering, North Carolina State University, Raleigh, North Carolina 27695-7907, United States.

These authors contributed equally to this work

* Corresponding authors: J. L. Jones (jacobjones@ncsu.edu) and K. Wang (wang-ke@tsinghua.edu.cn)

Abstract:

Excellent electromechanical properties have been reported in lead-free potassium sodium niobate (KNN)-based piezoelectric ceramics over the past 15 years. However, poor reproducibility of the electromechanical properties of KNN has been a major barrier to industrial development, due to a lack of full understanding of some of the processing aspects. Chemical inhomogeneity is one of the most critical challenges in processing, as the properties of KNN-based ceramics are strongly composition-dependent. In the present study, *in-situ* temperature-dependent X-ray diffraction and thermogravimetric analysis were employed to investigate the chemical reactions that occur during solid-state synthesis. Chemical homogeneity was found to be sensitive to the competition among reactants during synthesis. The phenomenon can reasonably explain the chemical inhomogeneity in KNN and possibly other lead-free piezoelectric ceramic systems prepared via solid-state synthesis.

Keywords: lead-free, potassium sodium niobate, ceramic, chemical inhomogeneity, solid-state reaction

1. Introduction

Piezoelectric materials are important functional materials for many areas, including aerospace, robotics, biomedical, and consumer electronic industries.[1-4] Lead zirconate titanate piezoelectric ceramics have been widely used in the industries since the mid-20th century, although they contain the Pb element which is harmful to both humans and the environment. Recently, many global governments have created regulations on the usage of lead-containing materials in electronics, *e.g.*, the well-known Restriction of Hazardous Substances (RoHS) directive in Europe.[5] After years of research, potassium sodium niobate ((K, Na)NbO₃, abbreviated as KNN) has been demonstrated to be a promising lead-free piezoelectric material for replacing lead zirconate titanate readily in certain applications.[6, 7]

Past research on KNN has been highly focused on the enhancement of piezoelectric coefficients.[8-13] Construction of a polymorphic phase boundary at around room temperature has been proposed to be an effective approach for enhancing piezoelectric coefficients.[14, 15] Generally, via chemical modification, longitudinal piezoelectric coefficients (d_{33}) ranging from 250 to 650 pC/N can be obtained in KNN-based ceramics, with corresponding Curie temperatures (T_c) ranging from 450 to 175 °C.[6] Even when certain compositions of KNN-based ceramics are shown to have exceptional piezoelectric coefficients, reproducing samples with similarly high piezoelectric coefficients has proven difficult, which hinders the adoption of these ceramics in industry and their production at larger scales.[16-18]

There are a number of reasons for why KNN-based ceramics with high piezoelectric coefficients are difficult to reproduce such as the hygroscopicity of carbonates,[19] volatilization of A-site elements,[20] stoichiometry,[21] liquid phase,[22] abnormal grain growth,[23] and chemical inhomogeneity.[24] Among these

issues, chemical inhomogeneity is arguably the most challenging. Wang *et al.* reported core-shell inhomogeneities in a Li and Ta co-doped KNN ceramic.[24] Several properties of the KNN ceramic were highly degraded due to the presence of the core-shell structure. However, Choi *et al.* manipulated a similar core-shell structure to achieve an extraordinary electric-field-induced strain (more than 1000 pm/V) in CaZrO₃ as well as Li and Ta co-doped KNN ceramics.[25] The underlying mechanism for the high electric-field-induced strain and the origin of the formation of the inhomogeneous structure so far remains unknown. Chemical inhomogeneity is still commonly reported in KNN-based ceramics.[26-28] We recently reported irregular grain growth in calcined KNN powder, which was accompanied by the coexistence of multiple ferroelectric phases in sintered ceramics when monoclinic niobium pentoxide (Nb₂O₅) was used as a reactant.[29, 30] The ferroelectric phase coexistence was rationalized by the chemical inhomogeneity of A-site elements, *i.e.*, K and Na, due to the poor chemical reaction during calcination.

To understand the origin of chemical inhomogeneity in KNN, *in-situ* temperature-dependent X-ray diffraction (XRD) and thermogravimetric analysis (TGA) were employed to characterize the chemical reaction during solid-state synthesis. In the present study, KNN powder was prepared via solid-state synthesis, by selecting different Nb₂O₅ reactants as an experimental variable, *i.e.*, orthorhombic and monoclinic Nb₂O₅. Additionally, a KNN-based composition that has recently been shown to exhibit improved piezoelectric coefficient, 0.92(K_{0.5}Na_{0.5})NbO₃-0.02(Bi_{0.5}Li_{0.5})TiO₃-0.06BaZrO₃ (abbreviated as BZ6), was prepared for comparison.[31, 32] Chemical inhomogeneity was observed in the calcined powder when the monoclinic Nb₂O₅ reactant was used, though it can be homogenized at high temperatures (above ~950 °C). A competitive reaction among carbonates with Nb₂O₅

was proposed to be the origin of the chemical inhomogeneity of calcined powder. Our results suggest that enhanced chemical homogeneity can be obtained if the competition among reactants during solid-state synthesis can be effectively avoided or mitigated.

2. Experimental

2.1 Preparation of powder mixtures

For the preparation of $(\text{K}, \text{Na})\text{NbO}_3$ (KNN) and $0.92(\text{K}_{0.5}\text{Na}_{0.5})\text{NbO}_3$ - $0.02(\text{Bi}_{0.5}\text{Li}_{0.5})\text{TiO}_3$ - 0.06BaZrO_3 (BZ6), raw materials including K_2CO_3 (99%, Sinopharm, China), Na_2CO_3 (99.8%, Sinopharm, China), Bi_2O_3 (99%, Sinopharm, China), Li_2CO_3 (99%, Sinopharm, China), TiO_2 (98%, Sinopharm, China), ZrO_2 (99%, Sinopharm, China), Ba_2CO_3 (99%, Sinopharm, China), Orthorhombic Nb_2O_5 (99.99%, Sinopharm, China), and Monoclinic Nb_2O_5 (99.95%, Conghua Tantalum and Niobium Smeltery, China) were used. When orthorhombic Nb_2O_5 was used as the reactant, the samples were labeled as “-O”, *i.e.*, KNN-O and BZ6-O. When monoclinic Nb_2O_5 was used as the reactant, the samples were labeled as “-M”, *i.e.*, KNN-M and BZ6-M. The raw materials were weighed according to the stoichiometric composition and subjected to ball milling at 300 rpm for 24 hours, with ZrO_2 balls and ethanol used as the milling medium and dispersant, respectively. Then, the mixtures were dried and sampled for the following characterization techniques.

2.2 Characterization of powder mixtures

The solid-state synthesis process was investigated by utilizing *in-situ* temperature-dependent XRD (Pixel1D, Empyrean, PANalytical) with high temperature chamber (HTK, Anton Paar)). The powder samples were heated with a heating rate of $1\text{ }^\circ\text{C}/\text{min}$ from RT to $650\text{ }^\circ\text{C}$, followed by a faster heating rate of $2.5\text{ }^\circ\text{C}/\text{min}$ up to

1100 °C. XRD patterns were measured continuously while heating. Peak fitting was done using Line-Profile Analysis Software (LIPRAS).[33] Thermogravimetric analysis (TGA) and differential thermal analysis (DTA) were undertaken by using a thermal analyzer (STA 449 F3 Jupiter, NETZSCH). Al₂O₃ crucibles were used. The powder samples were heated with a heating rate of 10 °C/min from 50 °C to 1150 °C. The derivative of TG (abbreviated as DTG) data was smoothed by using the Savitzky-Golay method with a polynomial order of 2.

2.3 Preparation and characterization of sintered BZ6 ceramics

The homogeneously mixed BZ6-O and BZ6-M raw powders were calcined in a furnace at 950 °C for 4 hours. Then, the calcined BZ6 powders were mixed with 2 wt% of MnO₂ (97.5%, Sinopharm, China) and subjected to another ball milling at 300 rpm for 24 hours. The MnO₂ was added as a sintering aid.[11] Later, the BZ6-O- 2wt% MnO₂ and BZ6-M- 2wt% MnO₂ powders were dried and pressed into compact discs of 1.5 mm thick and 10 mm in diameter. These discs were subjected to cold isostatic pressing at 200 MPa for 90 seconds before sintering at 1100-1160 °C for 4 hours. Samples sintered at 1100 °C were used in the subsequent characterization. For the scanning electron microscopy (SEM) imaging with secondary electron signals, the ceramics were mechanically polished and then thermally etched at around 1050 °C for 10 min. For the SEM imaging with backscattered electron signals and electron probe microanalysis (EPMA), the ceramics were only polished. The EPMA was conducted at 20 kV with 50 nA for 20 ms dwelling time. An area of 30 × 30 μm was measured with 250 × 250 points, equating to 0.12 μm/point. The EPMA results presented in the manuscript have been replotted with adjusted color bars for better presentation and the

original data can be found in the supplementary file. The experimental setup for the electrical measurement of sintered ceramics can be found elsewhere.[30]

3. Results and discussion

3.1 Formation of perovskite phases during calcination

The *in-situ* temperature-dependent XRD data from room temperature to 1100 °C for the KNN and BZ6 samples is shown in Fig. 1. Due to a greater scattering factor of the high-Z Nb with the incident X-ray, the diffraction signals of Nb₂O₅ reactants dominate the signal up to ~400 °C: the orthorhombic Nb₂O₅ can be observed in Fig. 1(a) and 1(c), while the monoclinic Nb₂O₅ can be observed in Fig. 1(b) and 1(d). For phase analysis of the Nb₂O₅ reactants, see Fig. S1(a) and S1(b).

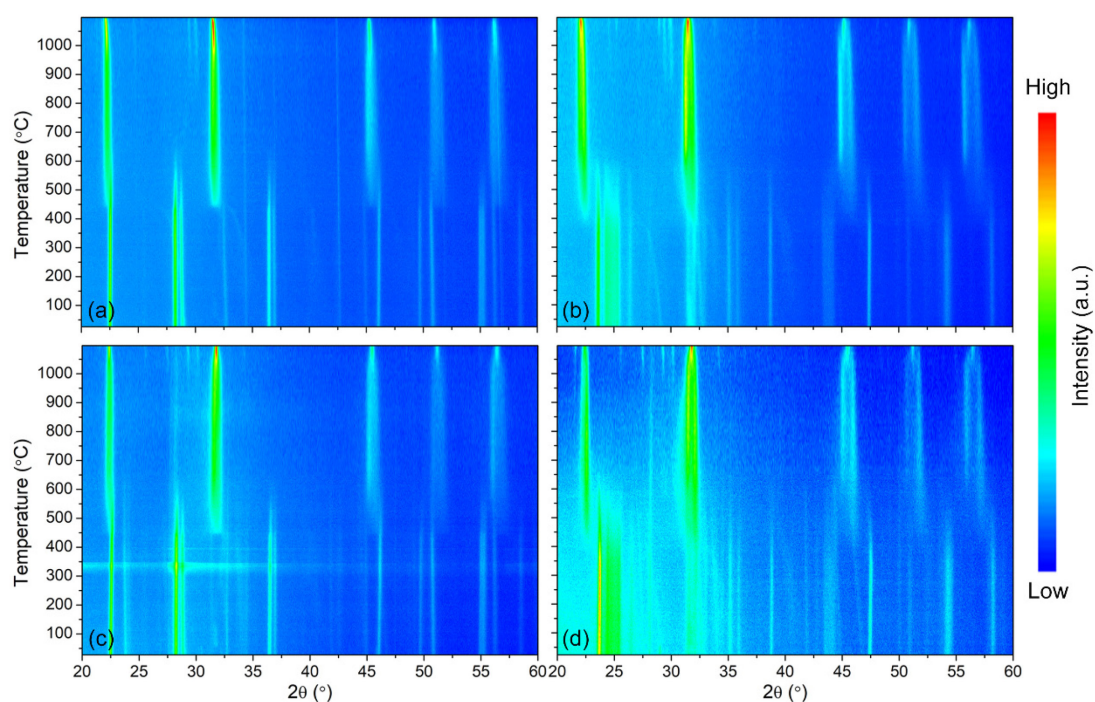


Fig 1. *In-situ* temperature-dependent XRD patterns of (a) KNN-O, (b) KNN-M, (c) BZ6-O, and (d) BZ6-M powder mixtures. An abnormal signal detected in the BZ6-O sample at ~350 °C is an occasional artifact due to surface misalignment, which is caused by the rapid emission of CO₂ during the decomposition of carbonates, see Fig. S2.

As the samples were heated above ~400 °C, the intensity of Nb₂O₅ gradually

decreased, accompanied by the formation of the perovskite phase. Peak labeling of the perovskite phase can be found in Fig. S1(c). The phase formation can be clearly observed in Fig. 2, which magnifies the 110_C reflection at 2θ ranging from 30 to 33.5° and temperature ranging from 250 °C to 650 °C. A subscript of “C” is used after the reflection index in this nomenclature to reference the cubic unit cell setting. It is observed that the formation temperatures of the perovskite phase vary among samples. For both KNN-O and BZ6-O, a broad diffraction peak located at $2\theta \sim 31.5^\circ$ formed near ~ 450 °C. In contrast, for KNN-M and BZ6-M, two diffraction peaks are observed, which indicates the formation of multiple perovskite phases of distinct lattice constants. Additionally, these perovskite phases sequentially formed with increasing temperature, where a perovskite phase located at $2\theta \sim 32^\circ$ formed at ~ 400 °C while the other one located at $2\theta \sim 31.5^\circ$ formed at ~ 450 °C. The coexistence of multiple phases in KNN-M and BZ6-M might indicate the chemical inhomogeneity of A-site elements in KNN perovskite.[28, 34]

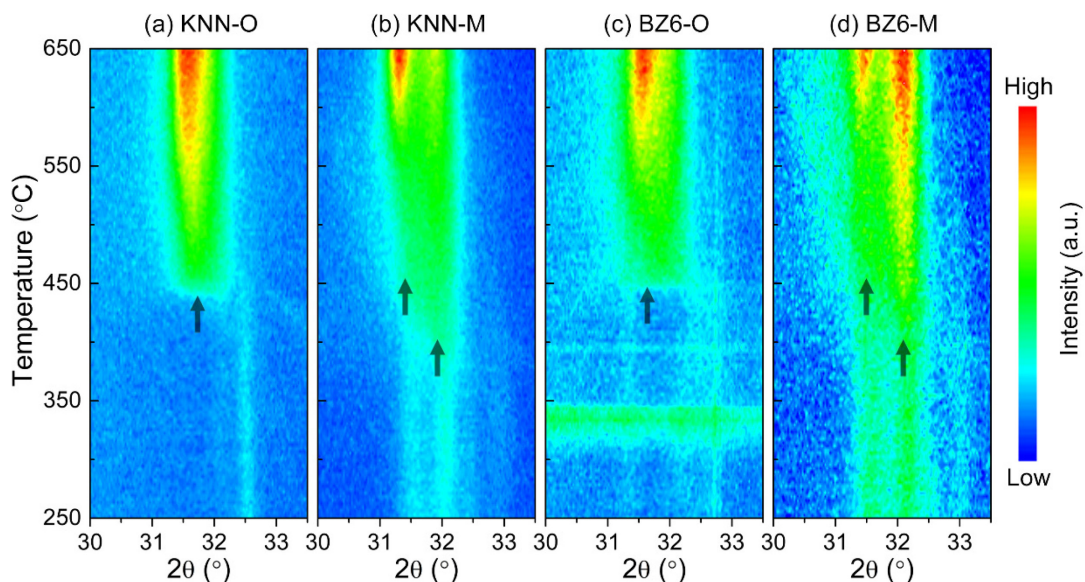


Fig. 2 *In-situ* temperature-dependent XRD patterns of (a) KNN-O, (b) KNN-M, (c) BZ6-O, and (d) BZ6-M powder mixtures, focusing on the 110_C reflection. The black arrows roughly identify the initiation of the formation of the perovskite phase.

A small amount of secondary phase was detected at high temperatures in all samples, which could be explained by the volatilization of alkaline elements. These secondary phases were conjectured to be non-perovskite, and mostly alkaline-deficient compounds, *e.g.*, $K_4Nb_6O_{17}$ or $Na_2Nb_4O_{11}$, which are common intermediate products.[35] However, since the diffraction intensity is low, it is difficult to identify the exact crystal structure of the secondary phase, see Fig. S1(d).

3.2 Chemical reaction among reactants during solid-state synthesis

The chemical reaction among reactants (or raw materials) during solid-state synthesis was further investigated by using TGA, as shown in Fig. 3. From Fig. 3(a), the thermogravimetric (TG) mass loss was found to gradually decrease with increasing temperature. The derivatives of TG mass loss (abbreviated as DTG) curves are shown in Fig. 3(b). Multiple DTG peaks are observed in different samples. TG mass loss can be explained by the volatilization of CO_2 during the decomposition of carbonates. The experimental TG mass losses are in agreement with the ideal volatilization of CO_2 from different carbonates, as summarized in Table 1. From the DTG curves, sequential decomposition of carbonates can be inferred. For KNN-O and BZ6-O, two overlapping DTG peaks can be located at ~ 500 °C and ~ 550 °C. However, for KNN-M and BZ6-M, two significant DTG peaks are located at more separated temperature regions, *i.e.*, ~ 470 °C and ~ 625 °C. There is another peak that occurs only in BZ6-O and BZ6-M at ~ 850 °C, which likely corresponds to the decomposition of $BaCO_3$. While most of the TG loss corresponds to the volatilization of CO_2 , a fraction of it might originate from the dehydration of hygroscopic carbonates, *i.e.*, the DTG peak at ~ 180 °C.[19]

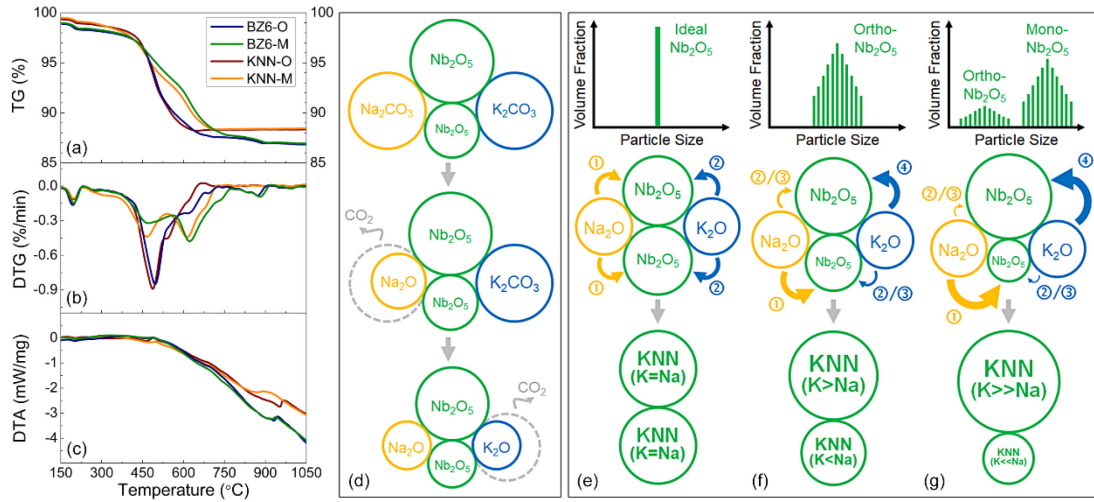


Fig. 3 TGA and DTA of different powder mixtures. (a) TG, (b) DTG, and (c) DTA. (d) Illustration of the sequential decomposition of carbonates. (e)-(g) Illustration of the chemical reaction of KNN when different Nb_2O_5 reactants are used: (e) ideal reactant with single particle size; (f) orthorhombic reactant with unimodal particle distribution; (g) monoclinic reactant with bimodal particle size distribution. The circled numbers and the thickness of the curved arrows represent the sequence of the reaction and the degree of reactivity between particles, respectively.

Table 1. Weight change expected from stoichiometric volatilization of CO_2 from different carbonates during the calcination of BZ6 and KNN powders.

Volatilization of CO_2	BZ6	KNN
K_2CO_3	5.05%	5.72%
Na_2CO_3	5.01%	5.67%
BaCO_3	1.32%	-
Li_2CO_3	0.11%	-
Total loss	11.49%	11.39%

In an experiment of diffusion couples between $\text{K}_2\text{CO}_3/\text{Nb}_2\text{O}_5$ and $\text{Na}_2\text{CO}_3/\text{Nb}_2\text{O}_5$ done by Malič *et al.*,^[35] the authors reported a higher reactivity rate in the $\text{Na}_2\text{CO}_3/\text{Nb}_2\text{O}_5$ couple than that in the $\text{K}_2\text{CO}_3/\text{Nb}_2\text{O}_5$ couple. The decomposition of the alkaline carbonates provides Na^+ or K^+ ions which then react with Nb_2O_5 . They suggested that Na_2CO_3 decomposes and reacts with Nb_2O_5 quicker than K_2CO_3 , as shown in Fig. 3(d). Based on their conclusion, we conjecture that the DTG peaks at low temperatures (~ 500 °C for KNN-O and BZ6-O; ~ 470 °C for KNN-M and BZ6-M) and

high temperatures (~ 550 °C for KNN-O and BZ6-O; ~ 625 °C for KNN-M and BZ6-M) correspond to the decomposition of Na_2CO_3 and K_2CO_3 , respectively. But now an interesting question arises: why do the DTG peaks vary when different Nb_2O_5 reactants are used? This is discussed below in section 3.3.

The DTA results are shown in Fig. 3(c). To state definitively whether a reaction is endothermic or exothermic from DTA data, a sample with a known thermal capacity is required to calculate a baseline. Since the thermal capacity of powder mixtures changes continuously throughout the solid-state synthesis due to the formation of KNN products during synthesis, it is difficult to obtain a baseline for subsequent quantitative analysis. Changes of thermal capacities are evidenced by the decreasing DTA curve starting from ~ 400 °C, when the solid-state reactions begin. The endothermic or exothermic peaks regarding the chemical reaction might be so low that are submerged by the decreasing DTA curve contributed from the changes of thermal capacities. If one can obtain a baseline based on reasonable prediction of the changes of thermal capacities, it is possible to extract the signal of endothermic/exothermic peaks for further analysis. As the changes of thermal capacities are assumed to be smooth and continuous, a rather significant change of the DTA data found at around 900 °C is possibly related to the chemical homogenization, and this is discussed below in section 3.4.

3.3 Size-dependent chemical reaction

The chemical reaction among reactants during solid-state synthesis is generally described as a diffusion process.[36, 37] For the synthesis of KNN, the chemical reaction might include the diffusion of cations (*i.e.*, K^+ , Na^+) into Nb_2O_5 , and the diffusion of O^{2-} anion in the same direction to maintain the electroneutrality.[35] The

diffusion kinetics depend on the chemical nature of the reactants and products, size distribution, shape, and uniformity of mixing, as well as the reaction processing parameters such as temperature, time, *etc.*[38]

To elucidate the impact of different Nb_2O_5 reactants on the chemical reaction, a qualitative model regarding size distribution is illustrated in Fig. 3(e-g). In this model, Nb_2O_5 powders of three different particle size distributions are considered. The chemical reactions among reactants during solid-state synthesis and the final KNN products are also shown in the figure. To explain the reaction during synthesis, four particles are sketched, including 2 particles in the middle that represent Nb_2O_5 ; the left and right particles represent Na_2CO_3 and K_2CO_3 , respectively. Both Na_2CO_3 and K_2CO_3 particles are closely connected with two Nb_2O_5 particles so that the Na_2CO_3 - Nb_2O_5 and K_2CO_3 - Nb_2O_5 reactions can both occur with equal probability. In other words, the reactants are assumed to be homogeneously mixed. Two KNN particles form as the final product and their K/Na ratios are highlighted.

First, we consider when an ideal Nb_2O_5 powder with single particle size is used as a reactant, as shown in Fig. 3(e). As previously mentioned, Nb_2O_5 could react quicker with Na_2CO_3 than K_2CO_3 . Since both Nb_2O_5 particles are of comparable size, the Na^+ ions would diffuse similarly onto both Nb_2O_5 particles, followed by a similar reaction for the diffusion of K^+ ions. Consequently, the K/Na ratio in two final KNN products would be equal to 1, which is an ideal case.

In many cases, the raw materials possess a unimodal particle size distribution, which will be discussed in the following scenario and is shown in Fig. 3(f). When a size discrepancy exists between two Nb_2O_5 particles, the Na^+ ions would react more quickly with the smaller Nb_2O_5 particle, due to the higher curvature, higher surface energy, and reduced diffusion distance.[38] The K^+ ions would also have a similar reaction with the

smaller Nb₂O₅ particle. However, the reaction between Na⁺ ions and the small Nb₂O₅ particles occurs so quickly that most of the Na⁺ ions would react with Nb and O to form a perovskite phase prior to K⁺ becoming available for the reaction. In parallel, only a small amount of Na⁺ ions would later react with the large Nb₂O₅ particle, as well as the remaining large amount of K⁺ ions. The reaction with the larger particle would occur at a higher temperature as compared with the smaller particle as it has lower surface energy and a longer diffusion distance. Consequently, the K/Na ratios of the final KNN products are different, where the smaller-particle and larger-particle KNN contain more Na or K, respectively. As mentioned in section 3.2, since the decomposition of the carbonates is required for the chemical reaction to occur, and herein the reaction is dependent on the size of the Nb₂O₅ particle, it is reasonable to expect sequential and slightly separated decomposition peaks in the DTG curve. Different decomposition behavior as a function of the size of the reactants was also reported in the preparation of BaTiO₃ from BaCO₃ and TiO₂.^[37] As the activation energy for the reaction depends on the size of the reactants, the required minimum reaction temperature would change accordingly.

Next, a Nb₂O₅ reactant with bimodal particle size distribution is considered, as shown in Fig. 3(g). The scenario is similar to the previous one, yet the competition for the reaction with Nb₂O₅ by K⁺ or Na⁺ is more extreme due to the larger size difference of the Nb₂O₅ particles. The final result is that more significant chemical inhomogeneity would be observed in the calcined KNN powder. Analogous to the previous scenario, a more intense competition during chemical reaction would reflect with remarkably separated DTG peaks.

The scenarios depicted in Fig. 3(f) and Fig. 3(g) are capable of explaining the situations when orthorhombic and monoclinic Nb₂O₅ are used, respectively. Thong *et*

al. have recently investigated the particle sizes of Nb₂O₅ reactants.[30] They found a homogeneous particle size distribution with an estimated average particle size roughly ~100 nm in orthorhombic Nb₂O₅ but a larger and inhomogeneous particle size distribution in monoclinic Nb₂O₅. Additionally, Hreščak *et al.* reported the appearance of nanocrystalline Nb₂O₅ up to 47% along with parent monoclinic Nb₂O₅ after ball milling.[39] The bimodal particle size distribution which consists of large monoclinic Nb₂O₅ and small nanocrystalline Nb₂O₅ might be able to explain the remarkably separated DTG peaks in the KNN-M and BZ6-M samples. Refer to Ref.[30] for a more complete description of particle size and morphology of Nb₂O₅ precursors and calcined KNN powder, including SEM images.

We note that the explanation of the size discrepancy of Nb₂O₅ was initially given by Hreščak *et al.*[39] Beyond the details of their explanation, we further elaborate on the competition among reactants during solid-state synthesis, with the support of *in-situ* temperature-dependent XRD and TG experimental data. Our model assumes that the competition during chemical reaction originates from the size discrepancy of Nb₂O₅ reactants, but it does not consider the chemical nature of different Nb₂O₅ reactants from the crystallography perspective, which would require further investigation. This model may also be applied to a relatively complex KNN-based system, since a size discrepancy among reactants may be encountered, *e.g.*, Nb₂O₅ and Ta₂O₅ in (K,Na)(Nb,Ta)O₃.

3.4 Chemical inhomogeneity and homogenization at high temperature

To further investigate the influence of temperature on the solid-state reaction of the powder mixtures, the XRD patterns measured at ~750 °C were examined, as shown in Fig. S3. The 110_c diffraction peaks of KNN-M and BZ6-M can be best fit using three

symmetric Lorentzian peaks, while the broad 110_c diffraction peak of KNN-O and BZ6-O can also be fit using two peaks, even though these peaks highly overlap with one another. It was previously mentioned that the resultant crystal structure of product KNN phases is strongly dependent on the K/Na ratio. Therefore, it is reasonable to conjecture that some level of chemical inhomogeneity occurs in all KNN and BZ6 samples. Intuitively, judging from the higher degree of peak splitting, KNN-M and BZ6-M are expected to have a more inhomogeneous chemical distribution than KNN-O and BZ6-O. A feasible way to examine this hypothesis is to increase the calcination temperature and to test if chemical homogenization occurs.

The homogenization of KNN and BZ6 samples at high temperature are shown in Fig. 4. For KNN-O and BZ6-O, as the temperature increases from 750 °C to 1100 °C, the broad 110_c peak slowly becomes a narrow peak with higher intensity at ~950 °C and ~1000 °C, respectively. For KNN-M and BZ6-M, with rising temperature, the separated 110_c peaks merge into a single yet broad peak at ~950 °C and ~1000 °C, respectively. The statistical fittings of 110_c peaks measured at ~1050 °C are again shown in Fig. S3. It is observed that KNN-O and BZ6-O can be fit with one peak but KNN-M and BZ6-M still exhibit multiple peaks. The fitting results indicate that some level of homogenization indeed occurs at high temperature for all samples. The chemical inhomogeneity in KNN-O and BZ6-O can be highly mitigated such that a single phase remains, while the homogenization efficiencies in KNN-M and BZ6-M are quite limited.

The homogenization of KNN perovskites with different K/Na ratios as a function of temperature is illustrated in Fig. 4(e) and 4(f). The formation temperature of K-rich and Na-rich KNN are assumed to be different, according to the experimental results previously mentioned. For KNN-O and BZ6-O, K-rich and Na-rich KNN can

inter-diffuse and form into KNN with a K/Na ratio of approximately 1. In contrast, for KNN-M and BZ6-M, since there is a significant compositional difference between K-rich and Na-rich KNN, the homogenization of these particles can still occur but with a limited efficiency, which consequently results in a KNN product with a wide K/Na ratio distribution.

Calcination around the homogenization temperature is highly recommended. However, the temperature should not be too high, considering that rapid grain growth at elevated temperatures would consume the driving force (*i.e.*, the surface energy) for homogenization, as discussed in our previous paper.[30] The most suitable calcination temperature (T_{cal}) for pure KNN is suggested to be 950 °C, while the T_{cal} for other modified KNN-based systems would require further investigation.

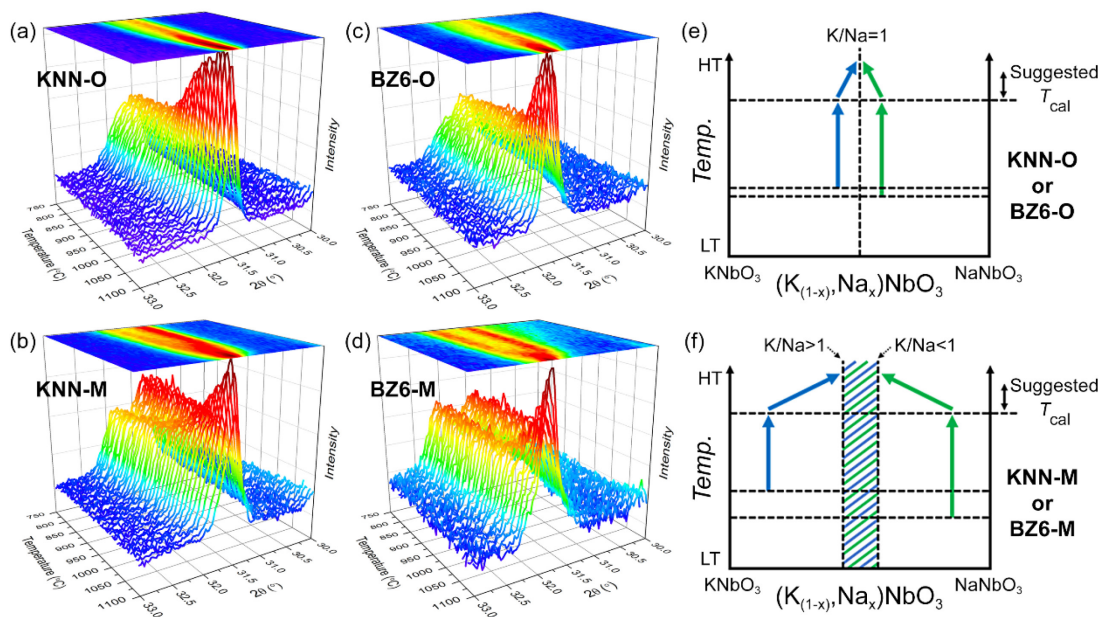


Fig. 4 *In-situ* temperature-dependent XRD patterns of (a) KNN-O, (b) KNN-M, (c) BZ6-O, and (d) BZ6-M powder mixtures at high temperature. A schematic view of the homogenization of perovskite phases for (e) KNN-O or BZ6-O and (f) KNN-M or BZ6-M at high temperatures. HT and LT represent high and low temperatures, respectively. T_{cal} represents the calcination temperature.

3.5 Chemical inhomogeneity in complex KNN-based composition

Chemical modification has been the most important approach for enhancing the piezoelectric coefficients of KNN-based piezoelectric materials. Multiple dopants (or modifiers) would be added to the KNN system simultaneously, which is now a common strategy in this research area.[6] Under such circumstances, the chemical reaction among reactants would become highly competitive. To understand the influence of competition among reactants on the final properties of sintered ceramics, BZ6 composition, a representative KNN-based composition which consists of 5 A-site elements and 3 B-site elements, were chosen for investigation. We prepared another two batches of BZ6-O and BZ6-M powder mixtures, instead of using the powder mixtures investigated by *in-situ* temperature-dependent XRD previously. The BZ6-O and BZ6-M powder mixtures were calcined at 950 °C for 4 hours in a box furnace and then mixed with sintering aid, *i.e.*, MnO₂, before sintering. The SEM images of calcined powders can be found in Fig. S4.

Dielectric, ferroelectric, and piezoelectric properties of the sintered BZ6-O and BZ6-M ceramics were measured, as shown in Fig. S5-S7. Both types of sintered ceramics were found to possess very similar properties. A slight difference was found between the Curie temperatures (T_C), where T_C of BZ6-M is higher than that of BZ6-O. For comparison, the characterization of sintered KNN-O and KNN-M ceramics can be found in our previous work.[30] Significant differences were found in the dielectric and ferroelectric properties of KNN-O and KNN-M ceramics, which is in contrast to BZ6 samples. Nevertheless, the T_C of KNN-M is also higher than that of KNN-O. It should be noted that KNN-O and KNN-M samples were calcined at 700 °C in the previous work, but BZ6-O and BZ6-M samples were calcined at 950 °C in the present study. Therefore, BZ6 samples should possess higher chemical homogeneity, which might explain the similarity in properties.

To examine the origin of the similarity in properties between BZ6-O and BZ6-M samples, their microstructures were investigated by using SEM and EPMA, as shown in Fig. 5. From the SEM images shown in Fig. 5 (a) and (c), the average grain sizes of both samples are found to be almost identical. From the EPMA results shown in Fig. 5(b) and (d), very similar chemical distributions are observed in both samples, which will be described in detail in the following paragraphs. Meanwhile, SEM-BSE was also measured, as shown in Fig. S8.

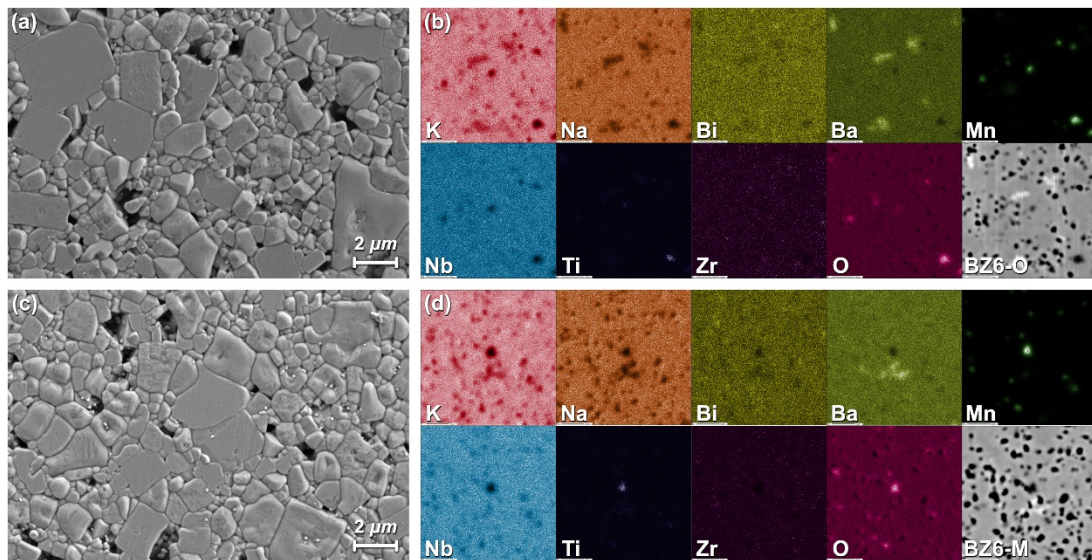


Fig. 5 SEM and EPMA results of sintered (a-b) BZ6-O and (c-d) BZ6-M ceramics. The EPMA figures are on a scale of $30 \times 30 \mu\text{m}$. The concentration of each element is proportional to the brightness of their corresponding colors. Note that the samples for SEM are polished and thermally etched while the samples for EPMA are only polished.

First, the back-scattered electron signal obtained from EPMA was presented in the bottom right of Fig. 5(b) and (d). Numerous dark regions were observed in both samples. In principle, the brightness contrast can be explained by the scattering of elements, orientation of grains, and the surface topology, *e.g.*, grains and pores. In these figures, the dark regions can be explained by the porosity of samples, but one should note that the area of these dark regions is apparently larger than that of the pores

observed in Fig. 5(a), Fig. 5(c), and Fig. S8 as well, which is mainly due to the poor focusing during the wavelength-dispersive spectroscopy (WDS) measurement. Despite the poor focusing, the WDS can normally probe into a depth of several μm from the surface, where the porosity will not affect the quality of images.

Comparing the chemical distribution of B-site elements, Nb and Zr share similar distribution while Ti segregates at some specific regions that coincide with the Mn distribution. Segregation of Mn at those specific regions indicates that Mn might have preferably substituted into the B site of the perovskite. Meanwhile, the excess Mn reacts with the substituted Ti and subsequently formed into a new secondary compound. A magnified EPMA result of Mn distribution can be found in Fig. S9, where a significant core-shell distribution is observed. The shell represents the region where Mn substituted into the B site of perovskite while the core represents the region where excess Mn formed into the secondary phase.

When comparing the chemical distribution of A-site elements, including K, Na, Bi, Li, and Ba, it is noted that Li is a very light element, which is undetectable in EPMA. It is observed that Bi is rather homogeneously distributed, compared to K, Na, and Ba. Although the distributions of K and Na are inhomogeneous, they almost overlap with each other. Broadly speaking, at the micrometer scale, the K/Na ratio in these regions could be approximately equal to 1. Still, the chemical homogeneity at the atomic scale requires further investigation. The overlapping of K and Na distributions likely originates from the homogenization during calcination at 950 °C.

The deficient regions in the K and Na distributions are unexpectedly complemented by the Ba distribution. We note that the decomposition of BaCO_3 occurs at a very high temperature, *i.e.*, ~ 850 °C, compared to that of the K_2CO_3 and Na_2CO_3 . Based on the explanation given in Fig. 3, the K_2CO_3 and Na_2CO_3 react with most of the

Nb_2O_5 at an early stage, while the BaCO_3 can only later react with the remaining (most likely large) particulates of unreacted Nb_2O_5 . The chemical inhomogeneity of Ba could undermine the properties of BZ6 considerably.

Our results demonstrate that the competition of reactants during the synthesis of KNN is decisive to the homogeneity and chemistry of the final products. The competition in KNN occurs among compounds containing A-site elements. Specifically, it occurs among carbonates like K_2CO_3 , Na_2CO_3 , and BaCO_3 , but not oxides like Bi_2O_3 . This is a unique processing issue for lead-free piezoelectric ceramics, as carbonates are not typically present in the preparation of lead zirconate titanate, rather oxides like PbO (or Pb_3O_4), ZrO_2 , and TiO_2 are used. Additionally, typical modifiers added to PZT are oxides as well, *e.g.*, MnO_2 , Fe_2O_3 , Nb_2O_5 , and La_2O_3 . Inferring from this, we expect that similar competitions could occur in many other lead-free piezoelectric ceramics, like BT-based[40] and BNT-based[41] systems. Take $\text{Ba}(\text{Zr}, \text{Ti})\text{O}_3$ - $(\text{Ba}, \text{Ca})\text{TiO}_3$ (abbreviated as BZT-BCT) for example,[42] BaCO_3 and CaCO_3 have the potential to compete with each other during the chemical reaction with ZrO_2 and TiO_2 ; while for $(\text{Bi}, \text{Na})\text{TiO}_3$ - $(\text{Bi}, \text{K})\text{TiO}_3$ - BaTiO_3 (abbreviated as BNT-BKT-BT),[43] competition could occur between Na_2CO_3 , K_2CO_3 , and Ba_2CO_3 . Nevertheless, homogenization could be done by controlling the processing conditions by choosing suitable reactants, optimizing the calcination (or homogenization) temperature, enhancing ball-milling efficiency to obtain smaller and homogeneous powder size, *etc.*

4. Conclusion

In the present study, a pure KNN and a complex KNN-based ceramic were prepared via solid-state synthesis by using the orthorhombic and monoclinic Nb_2O_5 reactants. The solid-state synthesis was investigated by *in-situ* temperature-dependent

XRD and TGA. From the XRD results, a broad 110_C peak was observed in KNN-O and BZ6-O, while two significantly separated 110_C peaks were observed in KNN-M and BZ6-M. The results indicate slight chemical inhomogeneity occurs in the former two and considerable inhomogeneity in the latter two samples. Meanwhile, from the TGA results, sequential decompositions of carbonates were observed in all samples. However, the temperature discrepancy of DTG peaks between Na_2CO_3 and K_2CO_3 in KNN-M and BZ6-M is larger than those in KNN-O and BZ6-O. It is suggested that the decompositions of carbonates depend on the size of the Nb_2O_5 reactant, as well as the chemical reactions. A qualitative model was provided to explain the chemical reaction and the resulted chemical distribution in calcined powder. By increasing the calcination temperature, chemical homogenization could be achieved yet the efficiency varies among samples. Finally, from the EPMA results of the sintered BZ6 ceramics, inhomogeneous chemical distribution of Ba was observed, which might originate from the late decomposition of BaCO_3 at $\sim 850^\circ\text{C}$. The results indicate that the competition among reactants during solid-state synthesis is a critical factor of processing. We proposed that the competition might explain the poor reproducibility of properties and performance in the KNN-based system, and a similar phenomenon could have occurred in other lead-free systems, where multiple reactants are used. If more uniformity of chemical distribution can be obtained, highly enhanced and reproducible properties and performance may be achieved.

5. Acknowledgements

This work was supported by National Nature Science Foundation of China (award number 52032005 and 51761135118), National Key Research and Development Program of China (award number 2020YFA0711700), and Beijing

Natural Science Foundation (award number JQ20009). The authors would like to acknowledge Prof. Jing-Feng Li for kindly providing experimental resources, Mr. Mao-Hua Zhang and Dr. Chunlin Zhao for many useful discussions. This work was performed in part at the Analytical Instrumentation Facility (AIF) at North Carolina State University, which is supported by the State of North Carolina and the National Science Foundation (award number ECCS-2025064). The AIF is a member of the North Carolina Research Triangle Nanotechnology Network (RTNN), a site in the National Nanotechnology Coordinated Infrastructure (NNCI). AP and JJ acknowledge partial support from the National Science Foundation (award number CMMI-1634955).

References:

- [1] M.T. Chorsi, E.J. Curry, H.T. Chorsi, R. Das, J. Baroody, P.K. Purohit, H. Ilies, T.D. Nguyen, Piezoelectric biomaterials for sensors and actuators, *Adv. Mater.* 31(1) (2019) 1802084.
- [2] N.T. Jafferis, E.F. Helbling, M. Karpelson, R.J. Wood, Untethered flight of an insect-sized flapping-wing microscale aerial vehicle, *Nature* 570(7762) (2019) 491-495.
- [3] K. Dong, X. Peng, Z.L. Wang, Fiber/fabric - based piezoelectric and triboelectric nanogenerators for flexible/stretchable and wearable electronics and artificial intelligence, *Adv. Mater.* 32(5) (2020) 1902549.
- [4] C. Qiu, B. Wang, N. Zhang, S. Zhang, J. Liu, D. Walker, Y. Wang, H. Tian, T.R. ShROUT, Z. Xu, Transparent ferroelectric crystals with ultrahigh piezoelectricity, *Nature* 577(7790) (2020) 350-354.
- [5] A.J. Bell, O. Deubzer, Lead-free piezoelectrics—The environmental and regulatory issues, *MRS Bull.* 43(8) (2018) 581-587.

- [6] H.-C. Thong, C. Zhao, Z. Zhou, C.-F. Wu, Y.-X. Liu, Z.-Z. Du, J.-F. Li, W. Gong, K. Wang, Technology transfer of lead-free (K, Na) NbO₃-based piezoelectric ceramics, *Mater. Today* 29 (2019) 37-48.
- [7] K. Shibata, R. Wang, T. Tou, J. Koruza, Applications of lead-free piezoelectric materials, *MRS Bull.* 43(8) (2018) 612-616.
- [8] H. Tao, H. Wu, Y. Liu, Y. Zhang, J. Wu, F. Li, X. Lyu, C. Zhao, D. Xiao, J. Zhu, Ultrahigh performance in lead-free piezoceramics utilizing a relaxor slush polar state with multiphase coexistence, *J. Am. Chem. Soc.* 141(35) (2019) 13987-13994.
- [9] Q. Liu, Y. Zhang, J. Gao, Z. Zhou, D. Yang, K.-Y. Lee, A. Studer, M. Hinterstein, K. Wang, X. Zhang, L. Li, J.-F. Li, Practical high-performance lead-free piezoelectrics: structural flexibility beyond utilizing multiphase coexistence, *Natl. Sci. Rev.* 7(2) (2020) 355-365.
- [10] T. Zheng, J. Wu, Electric field compensation effect driven strain temperature stability enhancement in potassium sodium niobate ceramics, *Acta Mater.* 182 (2020) 1-9.
- [11] M.-H. Zhang, K. Wang, Y.-J. Du, G. Dai, W. Sun, G. Li, D. Hu, H.C. Thong, C. Zhao, X.-Q. Xi, High and temperature-insensitive piezoelectric strain in alkali niobate lead-free perovskite, *J. Am. Chem. Soc.* 139(10) (2017) 3889-3895.
- [12] J. Fu, R. Zuo, Structural evidence for the polymorphic phase boundary in (Na, K) NbO₃ based perovskites close to the rhombohedral-tetragonal phase coexistence zone, *Acta Mater.* (2020).
- [13] P. Li, J. Zhai, B. Shen, S. Zhang, X. Li, F. Zhu, X. Zhang, Ultrahigh Piezoelectric Properties in Textured (K, Na) NbO₃ - Based Lead - Free Ceramics, *Adv. Mater.* 30(8) (2018) 1705171.
- [14] K. Wang, B. Malič, J. Wu, Shifting the phase boundary: potassium sodium niobate

derivates, MRS Bull. 43(8) (2018) 607-611.

[15] X. Lv, J. Zhu, D. Xiao, X.-x. Zhang, J. Wu, Emerging new phase boundary in potassium sodium-niobate based ceramics, Chem. Soc. Rev. 49(3) (2020) 671-707.

[16] J. Koruza, A.J. Bell, T. Frömling, K.G. Webber, K. Wang, J. Rödel, Requirements for the transfer of lead-free piezoceramics into application, J. Materiomics (2018).

[17] J. Rödel, K.G. Webber, R. Dittmer, W. Jo, M. Kimura, D. Damjanovic, Transferring lead-free piezoelectric ceramics into application, J. Eur. Ceram. Soc. 35(6) (2015) 1659-1681.

[18] B. Malič, J. Koruza, J. Hreščak, J. Bernard, K. Wang, J.G. Fisher, A. Benčan, Sintering of lead-free piezoelectric sodium potassium niobate ceramics, Materials 8(12) (2015) 8117-8146.

[19] N.M. Hagh, B. Jadidian, A. Safari, Property-processing relationship in lead-free (K, Na, Li) NbO₃-solid solution system, J. Electroceram. 18(3-4) (2007) 339-346.

[20] A. Popovič, L. Bencze, J. Koruza, B. Malič, Vapour pressure and mixing thermodynamic properties of the KNbO₃-NaNbO₃ system, RSC Adv. 5(93) (2015) 76249-76256.

[21] J. Acker, H. Kungl, M.J. Hoffmann, Influence of Alkaline and Niobium Excess on Sintering and Microstructure of Sodium - Potassium Niobate (K_{0.5}Na_{0.5})NbO₃, J. Am. Ceram. Soc. 93(5) (2010) 1270-1281.

[22] Y. Zhen, J.F. Li, Normal Sintering of (K, Na) NbO₃ - Based Ceramics: Influence of Sintering Temperature on Densification, Microstructure, and Electrical Properties, J. Am. Ceram. Soc. 89(12) (2006) 3669-3675.

[23] Y. Zhen, J.F. Li, Abnormal Grain Growth and New Core - Shell Structure in (K, Na) NbO₃ - Based Lead - Free Piezoelectric Ceramics, J. Am. Ceram. Soc. 90(11) (2007) 3496-3502.

- [24] Y. Wang, D. Damjanovic, N. Klein, E. Hollenstein, N. Setter, Compositional Inhomogeneity in Li - and Ta - Modified (K, Na) NbO₃ Ceramics, *J. Am. Ceram. Soc.* 90(11) (2007) 3485-3489.
- [25] S.-Y. Choi, S.-J. Jeong, D.-S. Lee, M.-S. Kim, J.-S. Lee, J.H. Cho, B.I. Kim, Y. Ikuhara, Gigantic electrostrain in duplex structured alkaline niobates, *Chem. Mater.* 24(17) (2012) 3363-3369.
- [26] O.A. Condurache, K. Radan, U. Prah, M. Otoničar, B. Kmet, G. Kapun, G. Dražić, B. Malič, A. Benčan, Heterogeneity Challenges in Multiple-Element-Modified Lead-Free Piezoelectric Ceramics, *Materials* 12(24) (2019) 4049.
- [27] J. Tangsritrakul, C. Tang, S. Day, D. Hall, Thermally-induced phase transformations in KNNS-BNKZ lead-free piezoceramics, *J. Eur. Ceram. Soc.* 40(3) (2020) 672-681.
- [28] M. Hinterstein, H. Mgbemere, M. Hoelzel, W. Rheinheimer, E. Adabifiroozjaei, P. Koshy, C. Sorrell, M. Hoffman, Influence of microstructure on symmetry determination of piezoceramics, *J. Appl. Crystallogr.* 51(3) (2018) 670-678.
- [29] H.-C. Thong, Z. Xu, C. Zhao, L.-Y. Lou, S. Chen, S.-Q. Zuo, J.-F. Li, K. Wang, Abnormal grain growth in (K, Na)NbO₃-based lead-free piezoceramic powders, *J. Am. Ceram. Soc.* 102(2) (2018) 836-844.
- [30] H.-C. Thong, C. Zhao, Z.-X. Zhu, X. Chen, J.-F. Li, K. Wang, The impact of chemical heterogeneity in lead-free (K, Na) NbO₃ piezoelectric perovskite: Ferroelectric phase coexistence, *Acta Mater.* 166 (2019) 551-559.
- [31] M.H. Zhang, K. Wang, J.S. Zhou, J.J. Zhou, X.C. Chu, X. Lv, J.G. Wu, J.F. Li, Thermally stable piezoelectric properties of (K, Na) NbO₃-based lead-free perovskite with rhombohedral-tetragonal coexisting phase, *Acta Mater.* 122 (2017) 344-351.
- [32] M.-H. Zhang, Y.-X. Liu, K. Wang, J. Koruza, J. Schultheiß, Origin of high

electromechanical properties in (K, Na) NbO₃-based lead-free piezoelectrics modified with BaZrO₃, *Physical Review Materials* 4(6) (2020) 064407.

[33] G. Esteves, K. Ramos, C.M. Fancher, J.L. Jones, LIPRAS: Line-profile analysis software, Preprint at https://www.researchgate.net/publication/316985889_LIPRAS_Line-Profile_Analysis_Software (2017).

[34] V.J. Tennery, K.W. Hang, Thermal and X - Ray diffraction studies of the NaNbO₃ - KNbO₃ system, *J. Appl. Phys.* 39(10) (1968) 4749-4753.

[35] B. Malic, D. Jenko, J. Holc, M. Hrovat, M. Kosec, Synthesis of sodium potassium niobate: a diffusion couples study, *J. Am. Ceram. Soc.* 91(6) (2008) 1916-1922.

[36] R.E. Carter, Kinetic model for solid - state reactions, *The Journal of Chemical Physics* 34(6) (1961) 2010-2015.

[37] M.T. Buscaglia, M. Bassoli, V. Buscaglia, R. Alessio, Solid - state synthesis of ultrafine BaTiO₃ powders from nanocrystalline BaCO₃ and TiO₂, *J. Am. Ceram. Soc.* 88(9) (2005) 2374-2379.

[38] M.N. Rahaman, *Ceramic processing and sintering*, CRC press, 2003.

[39] J. Hreščak, A. Bencan, T. Rojac, B. Malič, The influence of different niobium pentoxide precursors on the solid-state synthesis of potassium sodium niobate, *J. Eur. Ceram. Soc.* 33(15-16) (2013) 3065-3075.

[40] M. Acosta, N. Novak, V. Rojas, S. Patel, R. Vaish, J. Koruza, G. Rossetti Jr, J. Rödel, BaTiO₃-based piezoelectrics: Fundamentals, current status, and perspectives, *Appl. Phys. Rev.* 4(4) (2017) 041305.

[41] A.R. Paterson, H. Nagata, X. Tan, J.E. Daniels, M. Hinterstein, R. Ranjan, P.B. Groszewicz, W. Jo, J.L. Jones, Relaxor-ferroelectric transitions: Sodium bismuth titanate derivatives, *MRS Bull.* 43(8) (2018) 600-606.

[42] W. Liu, X. Ren, Large piezoelectric effect in Pb-free ceramics, *Phys. Rev. Lett.* 103(25) (2009) 257602.

[43] H. Nagata, M. Yoshida, Y. Makiuchi, T. Takenaka, Large piezoelectric constant and high Curie temperature of lead-free piezoelectric ceramic ternary system based on bismuth sodium titanate-bismuth potassium titanate-barium titanate near the morphotropic phase boundary, *Jpn. J. Appl. Phys.* 42(12R) (2003) 7401.